Generation of Orthomosaic Model for Construction Site using Unmanned Aerial Vehicle

Alexey Bulgakov[a], Daher Sayfeddine[a], Thomas Bock[b], Awny Fares[c]

[a]Department of Mechatronic, South Russian State Polytechnic University, Russia
[b]Department of Building Realisation and Robotics, Technical University of Munich, Germany
[c]Khatib Alami and Partners, Muscat, Oman
E-mail: agi.bulgakov@mail.ru, daher@live.ru, thomas.bock@br2.ar.tum.de, awny.fares@gmail.com

Abstract –

Researches on the combined platform of unmanned vehicles, especially aerial, and artificial intelligence can be executed on hobbyists' level with a low budget along with inside multi-billion-dollars technological laboratories. This flexibility has allowed UAV to attract financial potentials and even to migrate them from another technological field. Nowadays, UAVs are used in many industrial fields such as photogrammetry, cinematography, monitoring, cloud seeding. In this paper, we present our work on using UAV to generate a 3D model for a construction site. The purpose of the 3D model is to analyze day-by-day the development and progress on-site, to reconfirm the construction planning, discover opportunities and eliminate potential risks.

Keywords –

Construction site; Unmanned Aerial Vehicle; Artificial intelligence; 3D model

1 Introduction

There are different methodologies to generate 3D models. Mostly are based on Odometry and Photogrammetry algorithms [1-6]. The latter consists of obtaining information on a certain object by using recorded videos or pictures. The sources of the visual information vary depending on the purpose of the 3D model. For instance, it is possible to superimpose LIDAR scanning data [7-13] on infra-red and thermal pictures to detect cracks on the building and identify which construction material (type) has been exposed to damage. The value of photographic interpretation is well-founded in other medical and technical fields such as the Roentgen Stereo Photogrammetry. The application of this method in the construction field is called a computer stereo vision. It allows comparing information about a scene from two vantage points, for instance, obtained by satellite scanning and actual UAV recording.

The advantage of such an approach is to extract 3D information by examining the relative positions of the objects in two different panels. Often this method is used to assess a shore suffered previously by a damaging cyclone [6]. The hidden risk of micro motion displacement can only be identified many years later. Using the Stereo Photogrammetry on a frequent basis will allow the identification of such risks and mitigate them prior to their occurrence.

On the other hand, the inconvenience of using such a method is the embedded high cost and a huge amount of data to be stored and processed. Researchers in photogrammetry field are proposing a different solution for data compaction, however, most frequently the same is leading to decrease pictures quality, hence the generated model, or introducing additional processing noise due to combination of multiple algorithms and working desks.

For a construction field with a limited budget, the generation of a 3D photogrammetric model using UAV is cost-effective and serves the purpose of monitoring, activity planning, and progress control. In this paper, we present our work in generating a rendered 3D model based on orthomosaic and mesh model.

2 Mathematical foundation

In space, the unmanned aerial vehicle has six degrees of freedom, and its motion is described by six differential equations of motion (Euler equations). The solution of these equations in the general case would make it possible to determine the nature of the spatial motion of the UAV at any moment of time, and, in particular, defining the operator's influence on the controls, and would also make it possible to judge the stability of this flight.

However, the direct solution of these equations presents certain difficulties even when using modern computing machines. If we use a straight-line steady flight without sliding for the initial flight mode and consider the deviations of the motion parameters from the initial values to be sufficiently small, then due to the

symmetry of the UAV, the system of six equations of motion can be divided into two independent systems of equations that describe the motion of the UAV with an unknown degree of accuracy longitudinally and laterally.

It should be noted that for the photogrammetry task, the mathematical model will have three different referential axis systems (fig. 1): The Fixed-Earth system, the UAV or body-axis system, and the Camera system.

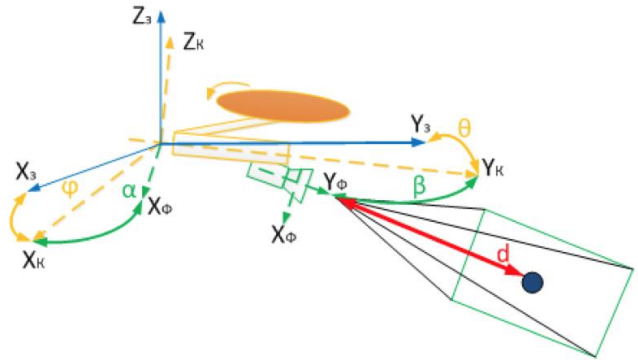

Figure 1. Representation of different systems for photogrammetry task

It is possible to establish mathematical equations for the transition between camera reference system and body-axis system. This is done using the following equations:

$$X_{\text{п}} = \frac{x}{\Pi x}.\cos\left(\arctan\left(\frac{H_B}{H_{\text{г}}}\right)\right); \quad (1)$$

$$Y_{\text{п}} = \frac{y}{\Pi y}.\sin\left(\arctan\left(\frac{H_B}{H_{\text{г}}}\right)\right),$$

$$\rho_x = \sqrt[2]{{X_{\text{п}}}^2 + {Y_{\text{п}}}^2} * cos(arctan\left(\frac{H_B}{H_{\text{г}}}\right)); \quad (2)$$

$$\rho_y = \sqrt[2]{{X_{\text{п}}}^2 + {Y_{\text{п}}}^2} * sin(arctan\left(\frac{H_B}{H_{\text{г}}}\right)).$$

Where, $X_{\text{п}}$ and $Y_{\text{п}} -$ are the pixel coordinates corresponding to linear motion, x and $y -$ are the Earth-Fixed axis coordinates; Πx and $\Pi y -$ are the scale coefficients, ρ_x and $\rho_y -$ are the pixel coordinates representing the rotational motion (roll and pitch angles); $H_{\text{г}}$ and $H_{\text{B}} -$ are the horizontal and vertical distance to Earth-axis coordinate in 2D mode.

3 Application of Photogrammetry

The following initial data were taken into consideration prior to launching the photogrammetry task. The construction plot is 416 Km^2, the average ground sampling distance or the distance between two consecutive pixel centers measured on the ground is 3.39 cm. The bigger the value of the image Ground Sampling Distance (GSD), the lower the spatial resolution of the image and the less visible details. The GSD is related to the flight height: the higher the altitude of the flight, the bigger the GSD value. The median of key points per image or the key points that are characteristic and can be detected on the images are 38981 key points per image. In total 1542 images were taken.

Based on equations (1) and (2), it could be retrieved that 1536 out of 1542 pictures could be processed considering the 60-degree angle introduced to install the camera on the UAV-axis. As such 0.94% relative difference between initial and optimized internal camera parameters can be computed (fig. 2).

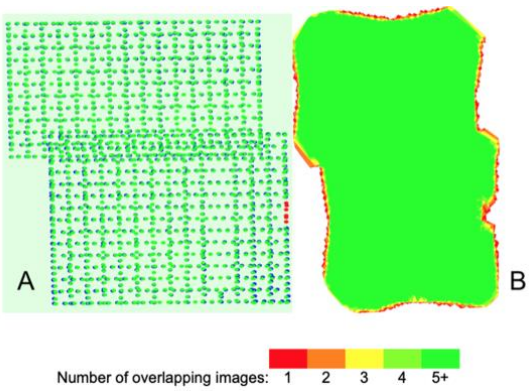

Figure 2. Offset results

Fig. 2 (A) shows the offset between initial (blue dots) and computed (green dots) image positions as well as the offset between the Ground Control Points (GCPs) initial positions (blue crosses) and their computed positions (green crosses) in the top-view (XY plane), front-view (XZ plane), and side-view (YZ plane). Red dots indicate disabled or uncalibrated images. Dark green ellipses indicate the absolute position uncertainty of the bundle block adjustment result. (B) shows the number of overlapping images computed for each pixel of the orthomosaic. Red and yellow areas indicate low overlap for which poor results may be generated. Green areas indicate an overlap of over 5 images for every pixel. Good quality results will be generated as long as the number of key point matches is also sufficient for these areas.

Fig. 3 shows the computed image positions with links between matched images. The darkness of the links indicates the number of matched 2D key points between the images. Bright links indicate weak links and require manual tie points or more images. The absolute geolocation variance shows the following:

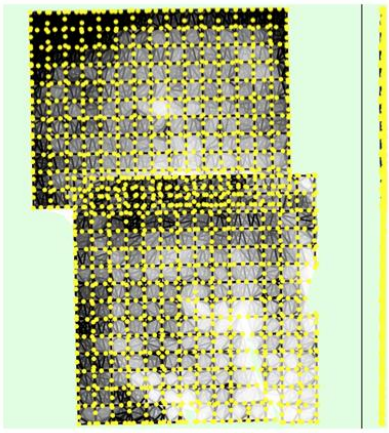

Figure 3. Links between matched images

Table 1. Absolute Geolocation Variance

Min Error [m]	**Max Error [m]**	**Geolocation Error x [%]**	**Geolocation Error y [%]**	**Geolocation Error z [%]**
-15	-12	0	0	0
-12	-9	0	0	0
-9	-6	0	0	0
-6	-3	0	0	0
-3	0	0.39	0	1.24
0	3	47.79	54.62	50.26
3	6	51.17	44.79	46.94
6	9	0.65	0.59	1.56
9	12	0	0	0
12	15	0	0	0
15	-	0	0	0
Mean [m]		**0**	**0**	**0**
Sigma [m]		**1.2513**	**1.2472**	**1.324**
RMS Error [m]		**1.2513**	**1.2472**	**1.324**

Where, Sigma is The standard deviation of the error in each direction (X,Y,Z) and RMS is the Root Mean Square error in each direction (X,Y,Z).

As the geolocation error is the difference between the initial and computed image positions, it should be stated that the image geolocation errors do not correspond to the accuracy of the observed 3D points. Min Error and Max Error represent geolocation error intervals between -1.5 and 1.5 times the maximum accuracy of all the images. Columns X, Y, Z show the percentage of images with geolocation errors within the predefined error intervals.

Table 2. Geolocation RMS Error

Geological Orientational Variance	RMS [degree]
Omega (roll)	2.006
Phi (Pitch)	1.901
Kappa (Yaw)	4.575

The geological orientational variance can be computed to define the Root Mean Square (RMS) in terms of degrees for the roll, pitch and yaw angles. Geolocation RMS error of the orientation angles identifies the difference between the initial and computed image orientation angles.

Figure 4. Orthomosaic Model of Construction Plot

4 Conlusion

The translating results from 2D orthomosaic to 3D Mesh shows several results. Firstly, as the proposed capturing angle is 60 degree and it is not assisted with any other capturing devices such as NADIR, the calibration of the images will be limited to the rendering algorithm. The first step is to produce mesh points obtained in Fig. 2 and Fig. 3 respectively. The result is shown in Fig. 5 along with the mesh textures.

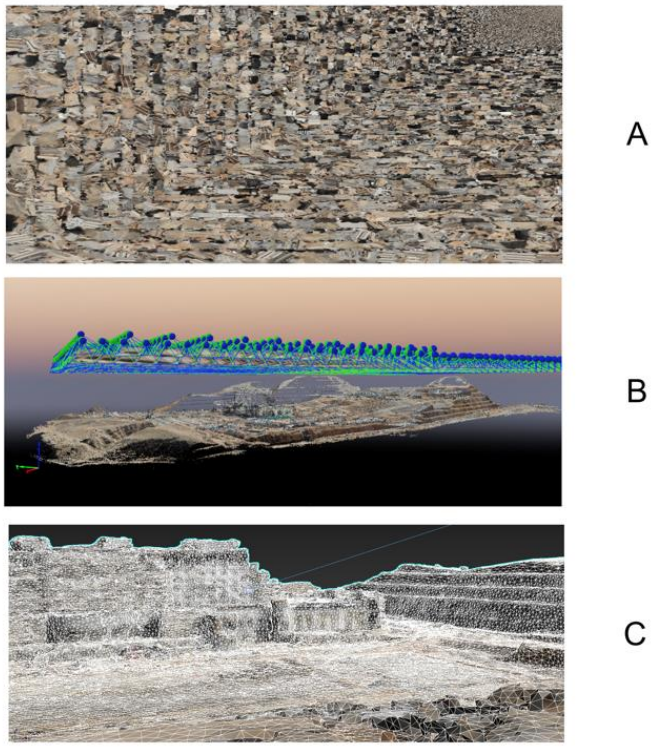

Figure 5. 3D Mesh and Texturing

The latter will be used to skin the mesh geometries, so the façades of the orthomosaic will reflect the actual status of the construction site. Lastly, the 3D model is rendered and illustrated in fig. 6.

Figure 6. Rendered 3D model

References

[1] Wierzbicki, D. Multi-Camera Imaging System for UAV Photogrammetry. 2018 Aug; 18(8): 2433.

[2] Guiseppina Vacca et al. The Use of Nadir and Oblique UAV Images for Building Knowledge. ISPRS Int. J. Geo-Inf. 2017, 6(12), 393

[3] Samad, A.M., Kamarulzaman, N., Hamdani, M.A., Mastor, T.A., Hashim, K.A. The potential of Unmanned Aerial Vehicle (UAV) for civilian and mapping application. In Proceedings of the IEEE 3rd International Conference on System Engineering and Technology (ICSET), Shah Alam, Malaysia, 19–20 August 2013; pp. 313–318

[4] Wang, C., Liu, X., Zhao, X., Wang, Y. An Effective Correction Method for Seriously Oblique Remote Sensing Images Based on Multi-View Simulation and a Piecewise Model. Sensors. 2016;16:1725. Doi: 10.3390/s16101725

[5] Hastedt H., Ekkela T., Luhmann T. Evaluation of the Quality of Action Cameras with Wide-Angle Lenses in UAV Photogrammetry. ISPRS-Int. Arch. Photogram. Remote Sens. Spat. Inf. Sci. 2016;XLI-B1:851–859.
Doi: 10.5194/isprsarchives-XLI-B1-851-2016

[6] Gonçalves, J.A., Henriques, R. UAV photogrammetry for topographic monitoring of coastal areas. ISPRS J. Photogramm. Remote Sens. 2015;104:101–111.
Doi: 10.1016/j.isprsjprs.2015.02.009

[7] Emelianov, S., Bulgakow, A., Sayfeddine, D. Aerial laser inspection of buildings facades using quadrotor. // Procedia Engineering, 85 (2014), pp. 140-146.

[8] Karabork, H., Sari, F. Generation of 3d city models from terrestrial laser scanning and aerial photography: A case study. 6 pages.

[9] Bulgakov, A., Evgenov, A., Weller, C. Automation high-rise structures inspection using quadrotor // Procedia Engineering, 123 (2015), pp. 101-109.

[10] Bulgakov, A., Sayfeddine, D., Otto, J., Emelianov, S. Dispersed cyber-physical coordination and path planning using unmanned aerial vehicle // Proceedings of the 36th International Symposium on Automation and Robotics in Construction (ISARC 2019). – Alberta: 2019, pp. 730-734.
DOI: https://doi.org/10.22260/ISARC2019/0098

[11] Kemper M. and Fatikow S. “Impact of center of gravity in quadrotor helicopter controller design,” in Proc. 4th IFAC-Symposium on Mechatronic Systems, (Heidelberg, Germany), 2006.

[12] Upadhay A. et al. UAV-Robot relationship for coordination of robots on a collision free path. International conference on robotics and smart manufacturing (RoSMa2018), pp. 424-431.

[13] Bertram, T., Bock, T., Bulgakov, A., Evgenov, A. Generation the 3D Model Building by Using the Quadcopter // 31st International Symposium on Automation and Robotics in Construction and Mining, 9-11 July 2014, Australia. – Sydney, University of Technology, 2014, pp. 778-783.